Linear stability analysis for an optimum Glauert rotor modelled by an actuator disc

D M Smith, H M Blackburn and J Sheridan

Monash University, Wellingon Road, Clayton Victoria Australia

E-mail: `david.m.smith@monash.edu.au`

Abstract.   We approximate a wind turbine using the Actuator Disc methodology with loading for an optimum Glauert rotor, and vary blade length and tip speed ratio, to determine base flows for linear stability computations at a Reynolds number of 100. Results from such computations suggest that the least stable mode is axisymmetric and insensitive to changes in tip speed operation, suggesting that the stability properties in the farfield wake for an optimised rotor are independent of the chosen tip speed optimization point. Higher azimuthal modes promote greater variation in velocities and may be relevant to cases at higher Reynolds numbers.

1. Introduction

Horizontal axis Wind Turbines (HAWT) continue to be a popular source of renewable energy, with total installed capacity growing. To minimise installed cost, turbines are sited in clusters or farms, where inflow conditions for some turbines can be subject to the wake of upstream turbines. A turbine wake is categorized into two parts; near and far wake. The near wake is similar in length to the rotor diameter, and blade properties such as circulation can be discerned. The flow structure of the near wake is three-dimensional and is described by a pair of helical vortices for each blade. The far wake follows the breakdown of the near wake and is approximately axisymmetric in the absence of an atmospheric boundary layer. Features of the far wake include a shear layer produced by the velocity deficit of the turbine, added swirl velocity and a higher turbulence intensity.

The increase in turbulence intensity and reduced flow velocities in the wake of a turbine are detrimental to turbines in the interior of a wind farm. The higher turbulence intensity leads to an increase in fatigue loading, and lower velocities lead to lower energy output. Under some freestream conditions where ambient turbulence is low, turbine wakes persist further into the wind farm, resulting in additional loading on turbines. Studies that draw links between ambient turbulence intensity and increased fatigue loading for wake sited turbines are given forthwith. Frandsen and Christensen in [3] observed an increased turbulence intensity owing to turbines operating in an upstream wake that were similar to a wind direction from land for the Vindeby offshore wind farm. A coastal wind farm was studied by Thomsen et al in [11] which identified that wake effects were more relevant in the fatigue loading for turbines when ambient turbulence intensity was low. The findings of Thomsen et al [11] are similar to the findings of Dahlberg et al in [6].

The observation that the turbulence created by the wake of a turbine can last a significant distance into a farm has produced renewed interest in the stability of flows related to turbine

wakes, particularly the helical vortex structure in the near wake. Widnalls' work [13] featured an inviscid helical vortex filament and identified the primary instability mechanisms as a short wave, long wave and mutual inductance modes. Widnall's findings were confirmed in a viscous setting by Walther et al [12]. Experimental investigations identify similar behaviour, including Felli et al [2], and also for turbine specific configurations by Nemes et al in [7]. The least stable mechanism identified by the above studies is the mutual inductance mode, where adjacent elements of the vortex filament are advected into one another, followed by merging and vortex breakdown.

It is unlikely for a turbine to be operating within the near wake of another turbine, and the far wake stability mechanisms are poorly understood by comparison to near wake instabilities. Additionally under some operating conditions, the three dimensional structure merges and forms an axisymmetric wake quickly, where modes for helical vortex structure may not significantly influence the wake dynamics. It is also unclear whether there is an interaction between root and tip structures with a corresponding influence on overall wake stability. To the authors' best knowledge, the stability of a flow produced by the Actuator Disc is yet to be considered. Given that axisymmetric models for turbines are also used for three dimensional computations wind farm scenarios, an understanding of the instability modes present for an axisymmetric approximation is of benefit with regards to interpretation of wind farm computations, however we note here that our investigation is limited by the absence of an atmospheric boundary layer.

In the present work we explore the wake stability of a Glauert optimum rotor modelled with an Actuator Disc as an approximation for a farfield turbine wake. The parameters considered include variations to the non-dimensional distance between blade root and tip, tip speed ratio, and the effect of swirl velocity on instability modes in a turbine wake.

2. Methodology
2.1. Nomenclature

|	
U_∞	Freestream velocity
$\lambda = R\Omega/U_\infty$	Tip speed ratio
Ω	Turbine angular rotation
Re	Reynolds number
R	Maximum turbine blade radius, measured from hub
r_0	Minimum turbine blade radius, measured from hub
ν	Kinematic viscosity
$\mathbf{u}$	Fluid velocity
x, r, z	Streamwise, radial, azimuthal directions
u, v, w	Velocity components: streamwise, radial, azimuthal
a	Streamwise induction factor
a'	Azimuthal induction factor
ϕ	Local blade angle of attack
F	Prandtls' tip loss factor
c	Local blade chord
C_n	Blade normal force coefficient
C_t	Blade tangential force coefficient
β	Azimuthal wavenumber

2.2. Problem parameters and domain
Base flows for stability analysis are calculated using the actuator disc concept, where axisymmetric turbine blade forces are introduced into computations via body forces in a spectral element Navier–Stokes solver. The two-dimensional base-flow calculations are performed for a domain with length scale defined by the rotor radius, and unit freestream velocity, resulting in

Reynolds number given by (1). Tip speed ratio is defined as the ratio of blade speed at the rotor tip to the freestream velocity in (1), expressed using blade angular rotation.

$$Re = \frac{U_\infty R}{\nu} \qquad \lambda = \frac{R\Omega}{U_\infty} \tag{1}$$

The cylindrical coordinate domain shown by figure 1 is a meridional semiplane, has rotor at the origin and comprises 2400 spectral elements with mapping in the turbine wake region to follow the turbine expanding wake. The cylindrical axis is aligned with the lower horizontal boundary, with flow from left to right. We specify a dirchlet inflow condition for the left boundary, free slip for the top boundary at maximum radial distance from the axis and neuman outflow condition for the outlet with zero dirchlet pressure. a High-order pressure boundary condition is used for the left and top boundaries.
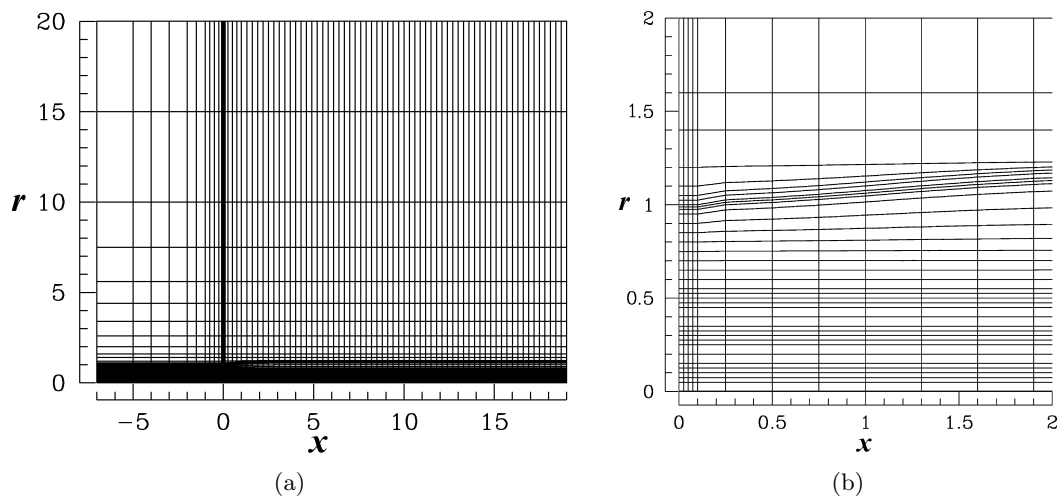
Figure 1. Computational domain showing spectral element boundaries with turbine hub located at (0,0) and extending to (0,1). 1(a): Computational domain. 1(b): subdomain showing refinement to local flow over the turbine and wake expansion.

2.3. Actuator Disc methodology
The axisymmetric Actuator Disc is part of a family of methods that can be considered as actuator Navier–Stokes methods, where the effects of the turbine are modelled via body forces. The Actuator Disc method was introduced by Sørensen and colleagues and is outlined by [10], [8] and [9]. Similar to the blade element momentum method, the turbine is discretized into a set of radial points at which the velocity is sampled. The local dynamic pressure at a given blade node is then used to scale force coefficients, providing a force, F_{2D} to be smoothed into the domain according to the smoothing kernel in (2), where d denotes the streamwise distance from the blade, r is the distance from the blade axis of rotation, and ϵ controls the width of the Gaussian kernel. As a result of the smoothing kernel, a forcing field $\mathbf{f}$ is available to be used to generate a base flow according to (3).

$$\mathbf{f}(d, r, z) = \frac{F_{2D}}{2\pi^{\frac{3}{2}} r \epsilon} \exp\left(\frac{-d^2}{2\epsilon^2}\right) \tag{2}$$

$$\frac{\partial \mathbf{u}}{\partial t} = \frac{-1}{\rho} \nabla p + \nu \nabla^2 \mathbf{u} - \mathbf{u} \cdot \nabla \mathbf{u} + \mathbf{f} \tag{3}$$

Force coefficients used in base flow computations are derived from an inviscid optimum Glauert rotor in [4], and are produced from streamwise and tangential induction factors a, and a' for such a rotor. The induction factors are defined by (4), which are subject to optimisation conditions provided in (5). The process is outlined by Hansen in [5].

$$a = 1 - \frac{u}{U_\infty} \qquad a' = \frac{w}{\Omega r} \tag{4}$$

$$\max\left(a'\left(1-a\right)\right) \qquad a' = \frac{1-3a}{4a-1} \tag{5}$$

To compute the magnitude of body forces in streamwise and tangential directions, we use the relationship between blade force and induction factor from the Blade Element Momentum method, given by (6) and compute the product of chord and force coefficient, in either rotor disc normal, cC_n, or tangential, cC_t directions inclusive of Prandtl's tip loss factor, F. Here, the angle of attack in the rotor blade normal plane is ϕ and the number of blades, B is three. The resulting forces in the base flow computation can be normalized using the local dynamic pressure.

$$\phi = \arctan\left(\frac{1-a}{1+a'}\Omega r\right) \qquad cC_N = \frac{4F\sin^2\phi}{\frac{B}{2\pi r}(\frac{1}{a}-1)} \qquad cC_T = \frac{4F\sin\phi\cos\phi}{\frac{B}{2\pi r}(\frac{1}{a'}+1)} \tag{6}$$

$$F = \frac{2}{\pi}\cos^{-1}\left(\exp\frac{-B(R-r)(1+\lambda^2)^{-0.5}}{2R}\right) \tag{7}$$

Comparisons of the base flows produced by the outlined actuator disc methodology have shown that for Reynolds numbers of $O(10^3)$, the streamwise flow at the rotor is within 5% of that predicted by the result of the optimization process described by (5), and that, as the Reynolds number is increased, to of $O(10^4)$, the agreement improves. We have chosen our smoothing kernel such that 95% of the smoothing forces are contained within the neighboring two elements of the blade. Variations to the smoothing kernel by a factor of two produce a change in velocity components of $O(10^{-5})$, for both velocities at the blade, and also in the wake.

2.4. Base flows and linear stability analysis

Here we present the parameter space and base flows for the linear stability analysis at a Reynolds number of 100 based from blade radius and methods used to measure the convergence of these flows to steady state. The optimum rotor was considered for tip speed ratios between 4 and 11. Blade spacings, r_0/R of 0.1, 0.3 and 0.5 were considered for the study. Given the preliminary nature of the study, only a Reynolds number of 100 was considered.

Convergence of base flows is measured by observing a residual, ς given by $\varsigma = \ln\left(|u(x,r,t+\delta t) - u(x,r,t)|/\delta t\right)$. We consider the flow to be converged when $\varsigma < -25$, implying changes in the baseflow of $O(10^{-12})$ for a given observation location of u. The residual also allows calculation of the least stable eigenvalue, as for a real valued eigenmode, it can be demonstrated that $\varsigma = at + c$ where a is the eigenvalue. Thus, axisymmetric growth rates are derived via fitting ς when the base flow is nearly converged. For computations of all eigenmodes and eigenvalues of non axisymmetric cases, the evolution of a white noise perturbation is considered via a linear operator by methods outlined by Barkley et al. in [1]. The modes computed by the linear stability analysis have the form $\mathbf{u(t)} = \mathbf{u_0}e^{\sigma t}$ where σ is the temporal growth rate and if positive indicates an unstable perturbation mode. Negative values for perturbation growth rates indicates that the base flow is stable. Given the linear nature of the analysis, it is possible to consider modes with varying azimuthal symmetry separately. Here we use the azimuthal

wavenumber, β to indicate the azimuthal variation of a mode shape over azimuth. $\beta = 0$ denotes an axisymmetric mode with zero variation over azimuth. Otherwise β indicates the number of periods over azimuth present for a perturbation.

Base flows can be described by a reduced velocity in the turbine wake with added swirl velocity produced by the turbine normal and tangential blade loading, with an example of a base flow given by figure 2(b), where streamwise velocity contours highlight root and tip shear layers. Variation in turbine loading with tip speed operation is shown by 2(a) where it can be observed that the optimum rotor has similar loading in the normal direction regardless of tip speed ratio. the only effect of λ is to modify the tip loss factor F and cause turbine normal loading at the tip to tend more gradually to zero for lower speed operation. The effect of λ on tangential velocity is more pronounced, with lower speeds giving rise to higher tangential loading and therefore higher swirl velocities in the wake. The cause of these changes is that the optimization process results in rotors that extract similar energy from the freestream and thus similar normal loading, however lower tip speed ratios result in flow in the rotor region more closely aligned with the freestream, and therefore the resulting lift force having larger proportion in the tangential direction.
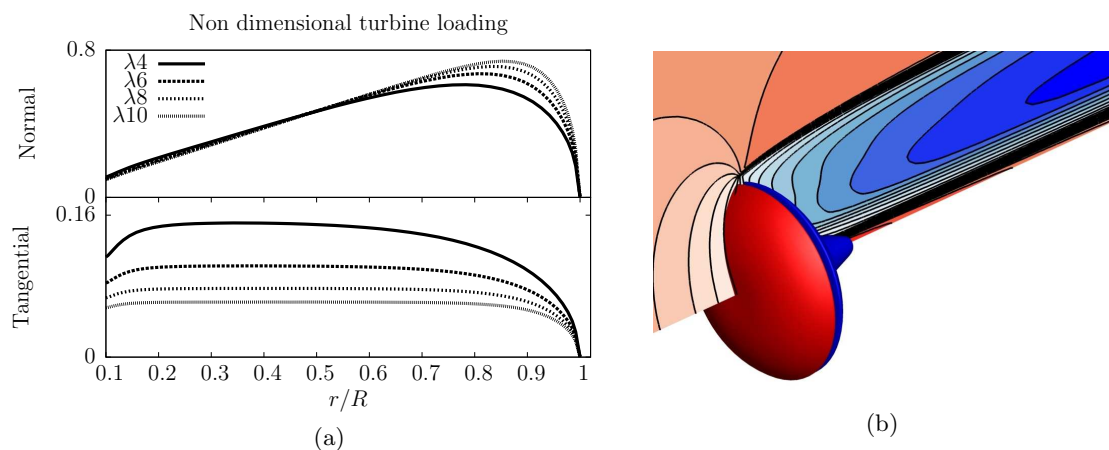
Figure 2. 2(a) Variation in turbine forces with tip speed ratio for steady state base flows at Re 100 with rotor spacing $r_0/R = 0.1$ 2(b) Base flow flowfield with meridional slice showing contours of streamwise velocity, with flow from left to right. Isosurfaces of pressure to indicate azimuthal symmetry and turbine location.

3. Results and Discussion

A summary for the growth rates for the study is given by figure 3 for the tip speed and geometry variations tested, and shows that the least stable modes observed were axisymmetric. In all cases observed, higher azimuthal wave numbers were progressively more stable. We also observe that, with the exception of a few cases, very little difference in growth rates is present, which is likely a consequence of very similar turbine normal loadings produced by the optimisation process. The primary cause of variation in turbine normal loading with tip speed operation is associated with Prandtl's tip loss factor, and therefore similar strengths of the shear layer are observed for a given turbine geometry. Different λ do however, alter turbine tangential loading more significantly, and therefore have more of an effect on the swirl velocity. The combined effect of minor changes to tip loading and swirl velocities that are an order of magnitude lower than freestream velocities accounts for the small variations in growth that have been observed.
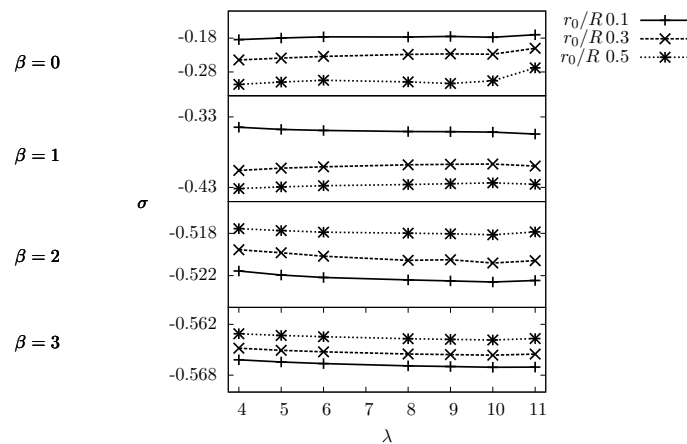
Figure 3. Variation of growth rates (σ) with respect to λ and blade root to tip spacing. From top to bottom: $\beta = 0$, $\beta = 1$, $\beta =, 2$ and $\beta = 3$.

Changes to turbine blade spacing, r_0/R have a more pronounced effect on wake stability, although these effects differ markedly for variations to the perturbation azimuthal symmetry. For axisymmetric and azimuthal wavenumber of unity, the least stable geometry is for r_0/R 0.1, however this trend is reversed for the remaining azimuthal wavenumbers. A longer blade, or lower r_0/R will produce a larger swept area, and therefore extract more energy than a similarly optimized, small blade. Therefore, smaller values of r_0/R affect the flow more strongly, and should be more susceptible to perturbations. Reasons for the inversion of this trend may be due to interaction between instabilities in the root and tip shear layers. We observe in figure 4(b) that localised structures are present near blade root and tip for azimuthal wavenumbers above zero. The interaction has not yet been explored in any depth, though may account for differences in r_0/R at higher azimuthal symmetries.
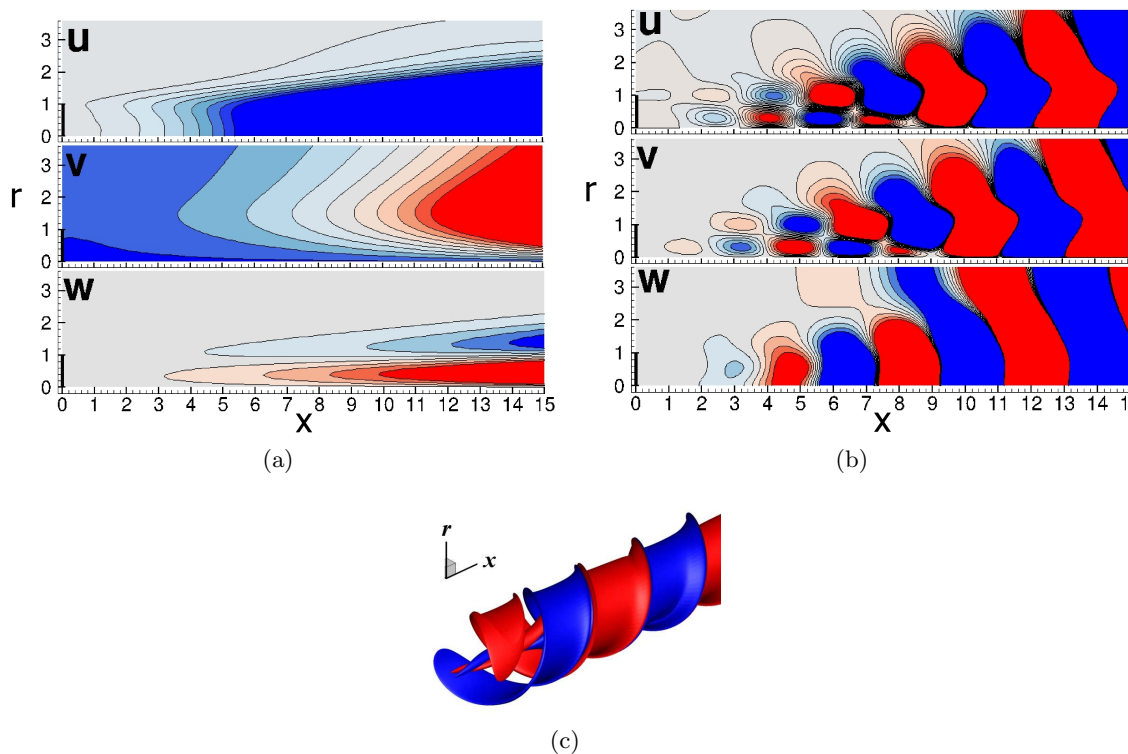
Figure 4. Least stable mode shapes shown via velocity components, with red/blue indicating positive/negative. Turbine, located at 0,0 and is highlighted with a solid line in a and b. 4(a) axisymmetric mode for blade spacing r_0/R 0.1 and $\lambda = 4$. 4(b) $\beta = 1$, $\lambda = 8$ and $r_0/R = 0.3$. 4(c) iso surfaces of streamwise velocity for leading mode $\beta = 1$, $r_0/R = 0.1$ and $\lambda = 8$ showing helical symmetry.

Mode shapes for the least stable modes are given by figure 4, where the axisymmetric mode is observed as a reduction in velocity for the wake and radial velocities acting to displace the shear layer radially outward. The perturbation may be the least stable configuration because it acts to increase the surface area of the shear layer, allowing for greater interaction with the freestream. Azimuthal velocities are also present for the axisymmetric mode, and shows significant radial variation. For higher azimuthal symmetry and above, it is clear that local structures act at the root and tip region for the turbine blade. Higher azimuthal modes also exhibit a streamwise periodicity. The $\beta = 1$ mode is characterised by streamwise velocities that alternately stretch or compress the shear layer, with regions where velocity is slowed corresponding with velocities radially inward from the freestream, which is reversed half a period later. The modes for $\beta = 1$ show helical symmetry when viewed in three dimensions which bears an interesting resemblance to the helical vortex structure of a real turbine wake. For higher azimuthal wavenumbers similar structures are observed to the mode for $\beta = 1$. The perturbation structures near root and tip shear layers grow in space and interact which is pronounced in the streamwise and radial velocities shown in figure 4(b). This type of behaviour may be responsible for the inverted trends with changed turbine blade length at higher azimuthal wavenumbers.

4. Conclusions

Inviscid calculations for an optimum Glauert rotor were used to prescribe turbine loading for an actuator disc simulation, which was then used as a steady state condition for the investigation of

instability mechanisms associated with the actuator disc approximation of a turbine. The least stable mode was identified for axisymmetric perturbations, and changes to tip speed operation did not significantly alter observed growth rates. Small variations in stability properties imply that provided a turbine is operating near its design condition, farfield stability properties are similar. For the least stable modes, shortening the blade length produced more stable wake states, though this was not the case for all azimuthal wavenumbers considered. A significant limitation of the present work is the small Reynolds number, and further works will consider how the findings presented here vary for higher Reynolds numbers.

References

[1] Dwight Barkley, HM Blackburn, and Spencer J Sherwin. Direct optimal growth analysis for timesteppers. *International Journal for Numerical Methods in Fluids*, 57(9):1435–1458, 2008.

[2] M. Felli, R. Camussi, and F. Di Felice. Mechanisms of evolution of the propeller wake in the transition and fa r fields. *Journal of Fluid Mechanics*, 1(1):1–49, 2011.

[3] S. Frandsen and C. J. Christensen. Vindeby offshore wind farm-fatigue loads. In *Contributions from the Department of Meteorology and Wind Energy to the EWEC'94 Conference in Thessaloniki, Greece*, page 107, 1995.

[4] H. Glauert. *Airplane Propellers*. Springer Berlin Heidelberg, 1935.

[5] Martin OL Hansen. *Aerodynamics of wind turbines*. Routledge, 2008.

[6] S. E. Thor J. Å Dahlberg, M. Poppen. Wind farm load spectra based on measurements. In *Proc. EWEA Special Topic Conf. 92: The potential of Wind Farms, Herning, Denmark*, 1992.

[7] A Nemes, M Sherry, D Lo Jacono123, HM Blackburn, and J Sheridan. Generation, evolution and breakdown of helical vortex wakes. 2012.

[8] Jens N Sørensen and Asger Myken. Unsteady actuator disc model for horizontal axis wind turbines. *Journal of Wind Engineering and Industrial Aerodynamics*, 39.

[9] Jens Nørkær Sørensen and Carsten Weber Kock. A model for unsteady rotor aerodynamics. *Journal of wind engineering and industrial aerodynamics*, 58(3):259–275, 1995.

[10] JN Sørensen, WZ Shen, and X Munduate. Analysis of wake states by a full-field actuator disc model. *Wind Energy*, 1(2):73–88, 1998.

[11] K. Thomsen, H. Bindner, T.F. Pedersen, and Test Station for Wind Turbines (Forskningscenter Risø). *Fatigue loads on a pitch regulated wind turbine operating in a coastal wind turbine array*. Risø National Laboratory, 1994.

[12] J. H. Walther, M. Guénot, E. Machefaux, J.T̃. Rasmussen, P. Chatelain, V. L. Okulov, J. N. Sørensen, M. Bergdorf, and P. Koumoutsakos. A numerical study of the stability of helical vortices using vortex m ethods. *Journal of Physics: Conference Series*, 75:012034, July 2007.

[13] S. E. Widnall. The stability of a helical vortex filament. *Journal of Fluid Mechanics*, 54(04):641, March 1972.